Advanced Steel Construction – Vol. 19 No. 2 (2023) 177–184
DOI: 10.18057/IJASC.2023.19.2.10

EXPERIMENTAL AND NUMERICAL ANALYSIS OF L-SHAPED COLUMN COMPOSED OF RECYCLED AGGREGATE CONCRETE-FILLED SQUARE STEEL TUBES UNDER ECCENTRIC COMPRESSION

Teng-Fei Ma [1, 2], Zhi-Hua Chen [1], Kashan Khan [1] and Yan-Sheng Du [1, *]

[1] *School of Civil Engineering, Tianjin University, Tianjin 300072, China*
[2] *Department of Civil Engineering, North China Institute of Aerospace Engineering, Langfang 065000, China*
** (Corresponding author: E-mail: duys@tju.edu.cn)*

ABSTRACT

The eccentric compression behaviors of L-shaped columns made of recycled aggregate concrete-filled square steel tubes (L-RACFST) with various replacement ratios of recycled coarse aggregate (RCA) are introduced in this paper. The experimental study demonstrates that the overall instability failure is the final failure mode of the L-RACFST columns and that the replacement ratio of RCA has little influence on the final failure mode of the specimens. When the RCA replacement ratio exceeds 40%, the specimens frequently move right into the failure stage. Recycled aggregate concrete (RAC) inside steel tubes can increase the load-carrying capacity and stiffness, preventing them from buckling inward compared to hollow steel tubes. The load-carrying capacity of the specimens gradually decreases as the replacement ratio of the RCA rises, and the ductility and stiffness deteriorate progressively. The bearing capacity declines more quickly, and the ductility coefficient and stiffness coefficient fall more slowly when the replacement ratio of RCA is higher than 40%. The bearing capacity of the specimens decreased by 29%, the ductility coefficient by 54%, and the stiffness coefficient by 60% as the replacement ratio of RCA increased from 0% to 100%. The specimen's ultimate strength decreases as the eccentricity rises. The numerical analysis results demonstrate that in the engineering design, the specimens' ultimate strength can be increased by strengthening the steel and raising the steel ratio; however, it is not advised to increase the connection plate's width to enhance the load-carrying capacity. The connection plate's primary function is to increase the stiffness of the steel surface and prevent local buckling, which has little bearing on improving the specimens' bearing capacity. It is advised that the replacement ratio of RCA in the L-RACFST columns should be less than 40% when considered with the research findings of reference [28].

ARTICLE HISTORY

Received: 31 August 2022
Revised: 9 February 2023
Accepted: 23 February 2023

KEYWORDS

Concrete-filled steel tube;
L-shaped column;
Recycled aggregate concrete;
Compression behaviour

1. Introduction

The use of steel structure homes has greatly accelerated the industrialization of building development in China. One of the most efficient ways to achieve building industrialization is to develop prefabricated construction. Recycled aggregate concrete (RAC), a green building material, can efficiently recognize the recyclability of waste concrete. With this method, resource recycling is feasible. Studies [1-4] show that RAC has low strength and significant creep shrinkage. Through experimental research, Wedding P A, Ridzuan A R M et al. [5–6] demonstrated that the strength of the RAC is decreased by 30% compared to natural concrete when the water and cement ratio is 0.35. The experiments conducted by Huda et al.[7] revealed that the mechanical properties of the RAC, such as the elastic modulus, strength, and Poisson ratio, decreased when compared to natural concrete. The impact of recycled coarse aggregates (RCA) of various ages on the resilience of RAC was investigated by Mahmood et al.[8].The findings indicate that when the replacement ratio of the RCA is less than 30%, its mechanical properties and durability are comparable to those of natural concrete. Shi et al. [9] .'s study of the mechanical properties and strength of the RAC with various RCA replacement ratios looked at the change law variation against time. The findings demonstrated that RAC with different RCA replacement ratios has lower density and strength than natural concrete.

According to some scholars, the RAC can be poured into steel tubes to produce recycled aggregate concrete-filled steel tubes (RACFST). Both the steel tube and the RAC are restrained. RAC and the benefits of steel tubes can both be utilized simultaneously [10–15]. Chen et al. [16] investigated the mechanical characteristics of the RAC-filled square steel tube columns using experimental research and numerical simulation. According to research findings, the bearing capacity slightly increases as the RCA replacement ratio rises. The failure mode of square steel tubes filled with RAC is comparable to that of square steel tubes filled with natural concrete. The compressive performance strength of steel tube columns filled with RAC under axial compression was investigated by Wang et al. [17]. The study's findings indicate that RACFST columns' compressive performance strength has decreased by less than 10%. In material tests, the strength reduction of the RACFST columns is less than that of the RAC samples. Tang et al. [18]'s study compared the seismic performance of steel tubes filled with natural concrete and those filled with RAC. This demonstrates that the seismic performance of the steel tube columns filled with RAC is comparable to that of the corresponding columns filled with natural concrete. The RAC-filled steel tube columns have a greater lateral bearing capacity and better ductility than the equivalent naturally concrete-filled steel tubular columns.

The home interior layout is restricted by the traditional square and rectangular section columns that protrude from the wall. A unique-shaped column made of square steel tubes filled with concrete (SCFST) can be concealed in a wall to increase the interior utilization space (Fig.1).

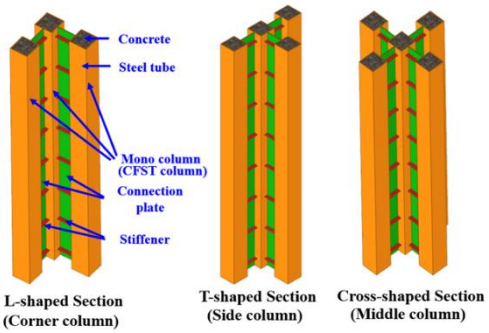

Fig. 1 The pecial-shaped column

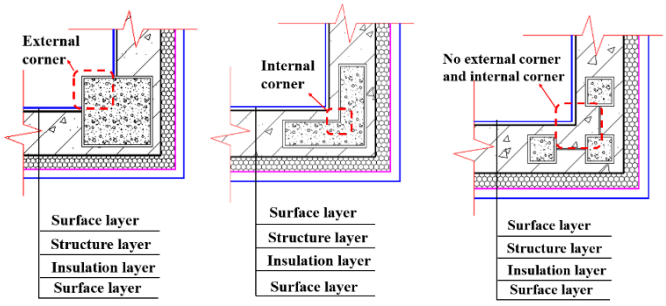

Fig. 2 The comparison of different types of columns

The L-shaped column comprises three square steel tubes filled with concrete that are joined together by stiffeners and connection plates. Connection plates' restricting impact on mono columns cannot be disregarded. The L-SCFST avoids internal corner folding compared to the L-shaped steel tube section column and does not lead to stress concentration (Fig.2).

Square concrete-filled steel tubular special-shaped (SCFST) column research has been conducted, but all of it is based on examining naturally concrete-filled square steel tubes. It was studied by Rong et al. [19–22] for its compressive properties under axial loads. The failure modes were also studied. The two types of failure that can occur in specimens with different slenderness ratios are strength failure and stability failure. The mechanical characteristics of hollow steel tubular special-shaped columns and SCFST columns were compared by Zhou et al. [23]. According to the study's findings, the SCFST's stiffness and bearing capacity are better than those of the hollow steel tube specimens. But its ductility was diminished. The eccentric mechanical behavior of the L-SCFST with various eccentricities was studied by Xu et al. [24]. The findings indicate that the specimen's bearing capacity decreases with increasing specimen eccentricity. The mechanical behavior of L-shaped columns made up of steel tubes filled with concrete that are connected by double vertical steel plates was investigated by Xiong et al. [25–27]. The findings demonstrate that the specimen transitions from a failure due to strength to an instability failure as the slenderness ratio increases under axial compression. The specimen's bearing capacity will significantly decrease as the eccentricity increases under the influence of the load.

The SCFST columns have great potential and can be used extensively in residential construction, whereas the RAC has not been employed to study behavior. The advantages of steel tubes and RAC can be fully utilized by recycled aggregate concrete-filled square steel tubes (RACFST); therefore, suggested in this paper. It can efficiently conserve indoor space, achieve resource recycling, encourage the transformation of buildings into low-carbon structures, and bring about the green development of buildings.

This study examined an L-shaped column of square steel tubes filled with recycled aggregate concrete (L-RACSFT). The L-RACFST columns, which are in a bidirectional bias state, are typically used as corner columns in engineering. The mechanical characteristics of the L-FACFST under eccentric compression are examined in this paper using various RCA displacement ratios. The effects of steel strength, steel ratio, eccentricity, and other factors on the mechanical properties of the L-RACFST columns are investigated through numerical simulation. The study's findings may serve as a theoretical basis for the L-RACFST columns' engineering design.

2. General situation of experiment

2.1. Specimens design and manufacture

The average building's story height in actual engineering is 3 m. The specimens created for this paper are limited by the test environment and are reduced by half scale, with the column height being taken as 1.5 m, the mono column's width being 100 mm, and its thickness being 3.75 mm. The connection plates have a 100 mm width and a 3.75 mm thickness. In Fig.3, the specimens' sizes are depicted. The specimens' ends' welding steel plates were measured as 20 mm. On the top steel plate, the load is applied. One hollow steel tube column was made as the comparison specimen to study how the RAC affected steel tubes. Table1 contains a list of the specimens' details. The L-RACFST columns' specifications also apply to hollow steel tube columns, except that no RAC is contained within them. The samples underwent a 28-day natural curing process. If the RAC sinks, it must be smoothed out with expanded mortar before welding the top cover plate.

Table 1
The specimens parameters

Specimens	Replacement ratio of RAC	Steel tube $h\times l\times t$ (mm)	Connection plate $l\times t$ (mm)	Eccentric distance(mm)
P40-0	0%	1500×100×3.75	100×3.75	40
P40-20	20%	1500×100×3.75	100×3.75	40
P40-40	40%	1500×100×3.75	100×3.75	40
P40-60	60%	1500×100×3.75	100×3.75	40
P40-80	80%	1500×100×3.75	100×3.75	40
P40-100	100%	1500×100×3.75	100×3.75	40
P40-K	--	1500×100×3.75	100×3.75	40

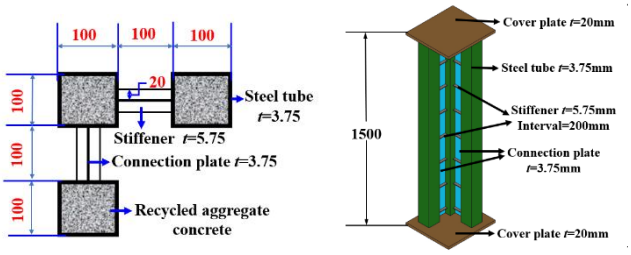

Fig. 3 Details of the L-shaped column (in mm)

2.2. Material properties

C30 natural concrete was used in this paper to form recycled aggregate concrete (RAC) using various ratios of recycled coarse aggregate (RCA) in place of natural coarse aggregate. Q235 is the strength grade of the steel, while to test the characteristics of RAC, concrete cubes were constructed.

Steel tubes, connection plates, and stiffeners were used as the sources for the samples of steel used to measure the properties of steel material. Additionally, the static test was used to determine the mechanical properties of the specimens subjected to the eccentric load discussed in this paper. Therefore, the RAC's strength and elastic modulus are primarily considered. This paper's material property test procedure follows the reference [28]. Three cubic blocks (100mm×100mm×100mm) and three prism blocks (150mm×150mm×300mm) for each RCA replacement ratio of RAC were tested to reduce the test error according to specification GB/T50081 [29]. The characteristics of RAC are listed in Table 2. Where $f_{c,cube}$ denotes the RAC's compressive strength in cubic units; $f_{c,prism,}$ shows RAC's compressive strength in prismatic units; and E_c represents the RAC's elasticity modulus. The strength and elastic modulus of the RAC gradually decline as the replacement ratio of the RCA rises. Table 3 provides a list of the steel's characteristics. Where $\boldsymbol{t}$ represents steel thickness, $\boldsymbol{f_y}$ denotes yield strength, $\boldsymbol{f_u}$ defines ultimate strength, and $\boldsymbol{E_s}$ indicates elastic modulus.

The reference[28] specifies the proportion of recycled concrete in the mix.

Table 2
The mechanical properties of RAC

Replacement ratio of RAC	$f_{c,cube}$(MPa)	$f_{c,prism}$(MPa)	E_c(MPa)
0%	33.36	26.7	32964
20%	29.00	25.8	23064
40%	17.59	14.0	13722
60%	13.30	12.2	14369
80%	11.94	10.0	10345
100%	8.99	8.4	9912

Table 3
The properties of the steel coupons

Material	t(mm)	f_y(MPa)	f_u(MPa)	E_s(MPa)
Steel tube	3.75	269	445	208,305
Connection plate	3.75	258	402	186,208
Stiffener	5.75	372	467	187,355

2.3. Loading point location

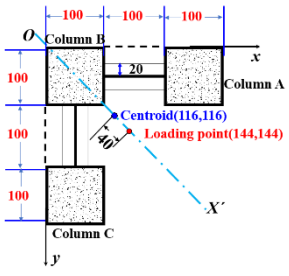

Fig. 4 Position diagram of the centroid and loading point(in mm)

The L-shaped columns, which have a bidirectional bias state, are typically used as corner columns. The ox's loading point was chosen for this study because it can recognize that the specimens are biased in both directions. The bearing capacity and ductility do not significantly decrease when the eccentricity is greater than 80 mm, according to the research findings of reference [24]. While studying the mechanical characteristics of the L-RACFST columns under various eccentricities, this paper uses the position with an eccentricity of 40 mm as the eccentric loading point and compares it to reference [28]. Fig. 4 depicts the loading point's position diagram. According to the source [28], the axial position of test specimens is calculated.

2.4. Experimental equipment and scheme

A 500T electro-hydraulic servo pressure test machine serves as the experimental apparatus. The L-RACFST column was placed on the pressure test machine's bottom plate and lined up its loading position with the machine's. While maintaining alignment between the pressure test machine's loading position and the special-shaped column's loading point, the L-RACFST column under the loading beam machine is prepared for loading. The L-shaped column has hinges at the top and bottom. The spherical hinge device, shown in Fig. 5, releases the restraint.

There are two stages to the loading process:

(1) Preloading: While ensuring the proper operation of the test machines, a preload of 100 kN was applied and maintained for 10 minutes. After that, the specimens were unloaded for formal loading.

(2) Formal loading: The method of gradual loading is used. A 200 kN force-controlled interval load was used and kept constant for 10 minutes before the specimens yielded. When the specimen yields, the loading is reduced by 100 kN in each successive step, and displacement control is applied.

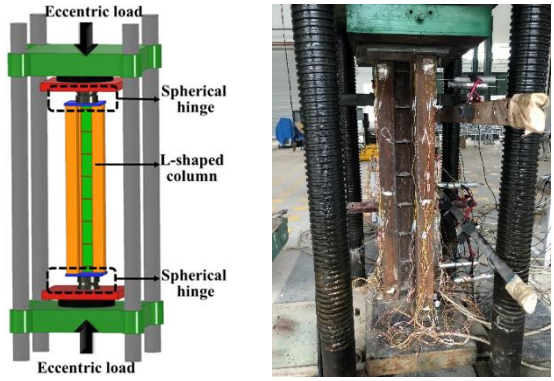

(a) Loading diagram (b) On-site photo

Fig. 5 Experimental equipment

2.5. Measurement arrangement

(1) Strain: The three mono columns were set up with strain gauges to measure the lateral and vertical strain of the steel tubes at the measurement points (see Fig. 6a).

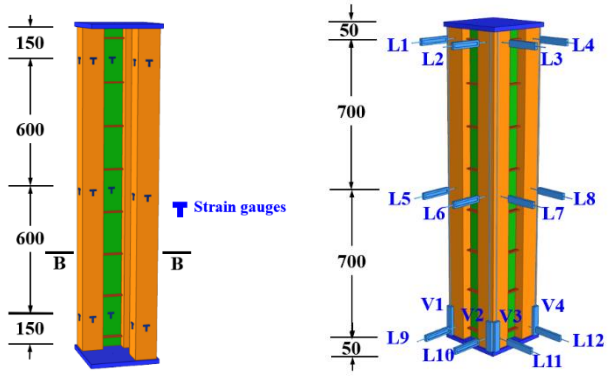

(a) Strain gauges (b) LVDT

Fig. 6 The layout of the measurement

(2) Displacement: Linear variable displacement transducers (LVDTs) are used to measure displacement. Twelve lateral LVDTs measured the specimens' lateral displacement at the column's top, middle, and bottom (L1-L12). Four vertical LVDTs (V1-V4) were used to measure the column's vertical displacement, as shown in Fig. 6(b).

3. Analysis of experimental phenomena and results analysis

3.1. Experimental phenomena

Similar experimental phenomena are observed in L-RACFST columns with various RCA replacement ratios. This suggests that the RCA's replacement ratio has little influence on experimental phenomena. The L-RACFST columns are bent and deformed with an angle to the weak axis. Both side mono columns (columns A and C) have distorted in a nearly symmetrical pattern. In general, column A and column C's deformation is greater than the corner mono column (column B). Local buckling of the specimens occurred within half of the top portion of the columns when the replacement ratio of RCA was 0% and 20%, respectively. Local buckling happened at the specimens' top or bottom when the RCA replacement ratio was greater than 40%. This is because the RAC filled in the steel tubes has low strength and high brittleness when the replacement ratio of RCA is greater than 40%. When the specimens are first loaded, the large cracks or compression will cause the RAC inside the steel tubes to quickly leave the work. Due to the lack of an effective RAC support inside, the top steel tubes would then buckle. However, the RAC filled inside the steel tubes has high strength and good ductility when the replacement ratio of RCA is between 0% and 20%. The steel tubes and the RAC filled inside of the steel tubes were stressed simultaneously during the initial stage of load application. The steel tubes are now holding the RAC in place to prevent it from being crushed. Meanwhile, the steel tubes' local buckling can be postponed by the RAC's efficient support for them. As the load grows, a portion of the RAC inside the steel tubes will separate from the work and become ineffective at supporting the steel tubes, which will cause localized buckling of the tubes. It is important to note that no local buckling on the surface joined to the connection plate, demonstrating that the stiffeners and connection plates increase the specimens' stiffness. During the test, it was discovered that some connecting plates were deformed along with the specimens' overall deformation, but this deformation had no impact on the specimens' overall deformation. The global instability failure of the L-RACFST columns is the last.

Local steel tube buckling is what ultimately causes hollow steel tubes to fail. This is due to the steel tubes' weak compression strength and the lack of an effective RAC support inside the hollow steel tubes. Thus, when the steel tubes experienced local buckling, the specimen could not support the load indefinitely, leading to ultimate failure. According to this, the RAC inside the steel tubes keeps them from buckling inward and improves the stiffness of the L-RACFST columns. Fig.7 depicts the L-RACFST columns' failure mode.

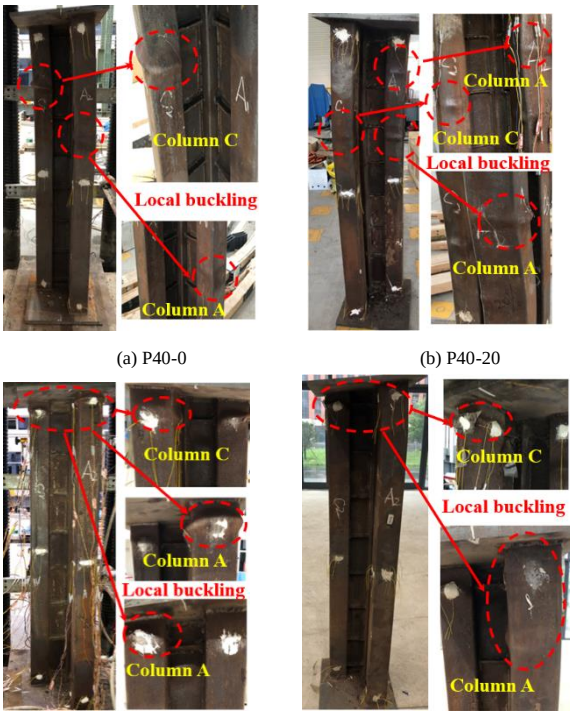

(a) P40-0 (b) P40-20

(c) P40-40 (d) P40-60

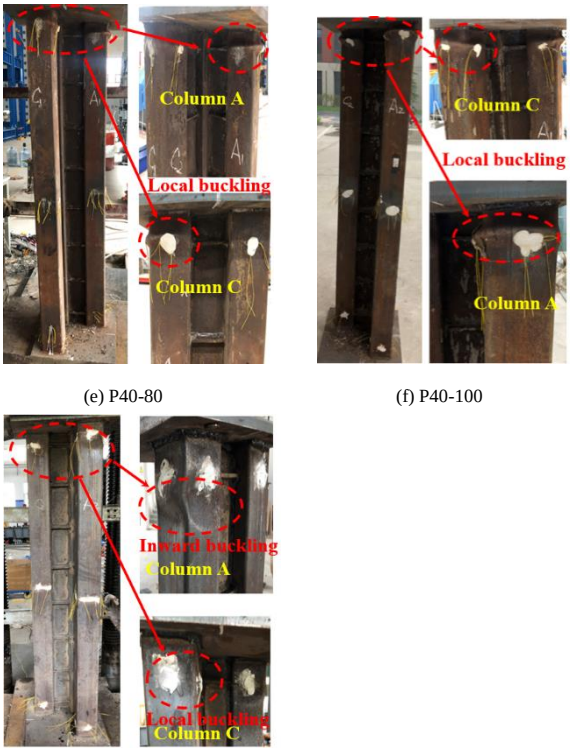

(e) P40-80 (f) P40-100

(g) P40-K

Fig. 7 Failure mode of the L-RACFST columns

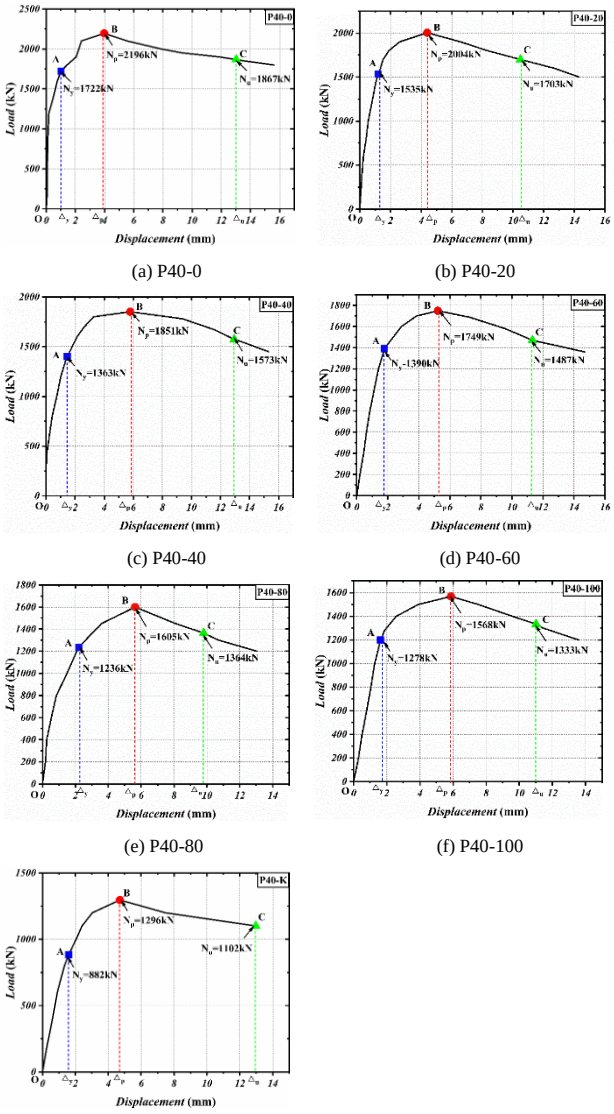

(a) P40-0 (b) P40-20

(c) P40-40 (d) P40-60

(e) P40-80 (f) P40-100

(g) P40-K

Fig. 8 Load-displacement curve

Fig. 8 displays the load-displacement curves. The yield load is denoted by A, the peak load point is pointed at B, and the ultimate load point is C. The "farthest point method" can determine the yield load point, which is the critical point between the elastic and elastic-plastic stages [30]. The test procedure can be divided into three stages, as shown by the curve: the elastic, elastoplastic, and plastic stages.

(1) Elastic state (OA section) is the region from the initial loading to the yield load. The load-vertical displacement curve exhibits linear behavior at this point. The RAC and steel tubes operate separately and without interactions. Vertical deformation is present in RAC and steel tubes alike. The connection plate does not restrain the steel tubes. In Fig. 9(a), the deformation diagram is displayed.

(2) Elastoplastic stage (AB section) extends from yielding to the peak load. The load-displacement curve exhibits a softening behavior at this point. The steel tubes and RAC interact; as the lateral deformation of the concrete increases, the steel tubes are constrained from buckling inward. The steel tubes also prevent the RAC from producing excessive deformation, which delays the crushing process. Numerous stress redistribution processes between steel tubes and RAC culminate in deformation coordination. The connection plate also restrains the steel tubes. In Fig. 9(b), the deformation diagram is displayed.

(3) Plastic stage (BC section) occurs when the load starts to decline after reaching its ultimate load. The load-displacement curve displays a descending branch at this point. Higher stress causes the RAC to deform significantly and become crushed. Depending on the RAC failure mode, there are various supporting effects on the steel tubes. As a result, the L-RACFST columns' plastic section is unique.

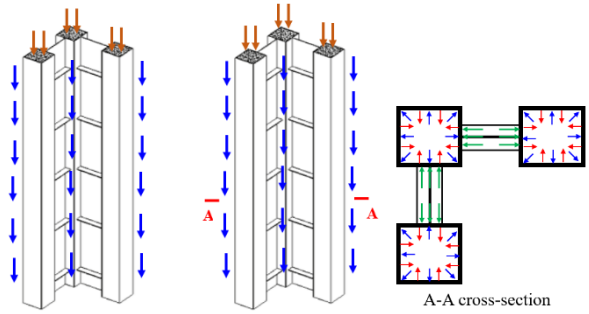

(a) Elastic stage (b) Elastoplastic stage

Fig. 9 Deformation diagram

The L-RACFST columns enter the failure stage immediately during the test when the replacement ratio of RCA is greater than 40%. It suggests that the ductility is deteriorating. The reason is that the strength and elastic modulus of the RAC gradually decrease as the replacement ratio of the RCA rises. As a result, as the load increases, the maximum load that the RAC inside the steel tubes can support gradually declines. Additionally, the steel tubes' ability to support a load for a shorter period decreases as RAC strength increases inside the steel tubes. The load-vertical displacement curve analysis's findings align with the phenomena observed in experiments.

3.2. Analysis of the experimental results

3.2.1. Bearing capacity

Table 4 displays the feature points of the load displacement data. The peak load gradually decreases as the replacement ratio of RCA rises. The reduction ratio of load of the L-RACFST columns compared to the specimen with a 0% RCA replacement ratio is shown in Table 5. Fig. 10 depicts the bearing capacity change curve with the replacement ratio change. The yield load and peak load decreased by 15.71% and 20.85%, respectively, as the replacement ratio of RCA increased from 0% to 40%. However, the RAC's cubic compressive strength fell by 47.27%. Peak load decreased by 28.60%, and yield load by 25.78% as the replacement ratio of RAC increased from 0% to 100%. However, the RAC's cubic compressive strength dropped by 73.05%. It is clear that RAC materials' strength reduction is much greater than the strength reduction of L-RACFST columns. This demonstrates that when RAC is injected into steel tubes, the steel tubes will restrain the RAC, allowing the benefits of both steel tubes and RAC to be utilized.

The yield load and peak load of the L-RACFST columns decrease more quickly when the RAC replacement ratio is higher than 40%, as seen from a comparison of the load value results.

Table 4
The load and displacement information of the specimens

Speci-mens	Yield point		Peak point		Ultimate point		*DI*	S_y
	Δ_y /mm	N_y /kN	Δ_p /mm	N_p /kN	Δ_u /mm	N_u /kN		
P40-0	1.01	1722	3.97	2196	13.03	1867	12.90	1705
P40-20	1.20	1535	4.39	2004	10.45	1703	8.71	1279
P40-40	1.35	1363	5.78	1851	12.95	1573	9.59	1010
P40-60	1.79	1390	5.23	1749	11.12	1487	6.21	777
P40-80	2.20	1236	5.63	1605	9.80	1364	4.45	562
P40-100	1.86	1278	5.88	1568	11.02	1333	5.92	687
P40-K	1.59	882	4.71	1296	12.97	1102	--	--

Table 5
The date of the specimens(comparison with P40-0)

Speci-mens	N_y /kN	Reduce proportion	Np /kN	Reduce proportion	N_u /kN	Reduce proportion
P40-0	1722	--	2196	--	1867	--
P40-20	1535	10.86%	2004	8.74%	1703	8.78%
P40-40	1363	20.85%	1851	15.71%	1573	15.75%
P40-60	1390	19.28%	1749	20.36%	1487	20.35%
P40-100	1278	25.78%	1568	28.60%	1333	28.60%
P40-K	882	48.78%	1296	40.98%	1102	40.97%

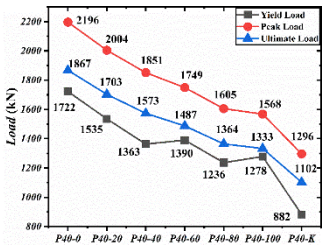

Fig. 10 Bearing capacity

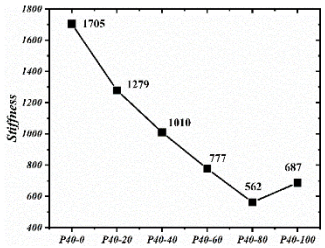

Fig. 11 Stiffness

3.2.2. stiffness

The ability of a material to resist elastic deformation when applied with force is referred to as stiffness. It represents the difficulty of elastomeric material deformation. The stiffness performance of the specimens in this paper is described using the secant stiffness (S_y) coefficient.

In Equation (1), where y is the vertical displacement of the specimens when the load reaches the yield load, the secant stiffness (S_y) of the yield point was used to characterize the stiffness of the L-RACSFT columns.

N_y is the specimens' yield load.

$$S_y = \frac{N_y}{\Delta_y} \tag{1}$$

Table 4 displays the S_y data. Fig. 11 depicts the stiffness coefficient-displacement ratio curve. The stiffness decreases by about 41% as the RCA replacement ratio rises from 0% to 40%. The stiffness decreases by about 60% as the RAC replacement ratio increases from 0% to 100%. The L-RACFST column's stiffness (RCA replacement ratio of 0%) is lower than the L-SFCST column's stiffness. The stiffness of the L-RACFST columns gradually decreases as the replacement ratio of RCA rises. This demonstrates that the specimens' resistance to elastic deformation is weaker the higher the replacement ratio of the RCA of the RAC. This is because the RAC's ductility in steel tubes decreases, and its exit from service accelerates with increasing RCA replacement ratios.

3.2.3. ductility

When a material exhibits ductility, it can fully exert its plastic deformation capacity while maintaining its bearing capacity even after it has reached its yield load. Evaluating the structure's seismic performance is very important. In this paper, the ductility performance of the specimens is described using the Secant Ductility Index (DI).

The secant ductility index (DI), which is defined as Equation (2), is used to characterize the ductility of the L-RACFST columns.

$$DI = \frac{\Delta_u}{\Delta_y} \tag{2}$$

where, Δ_u denotes axial shortening at the ultimate load. Δ_y represents vertical displacement at the yield load.

Fig. 12 displays the ductility index-displacement ratio curve. The L-RACFST columns are less ductile than the L-SFCST ones. The ductility decreases by about 54% as the replacement ratio of RCA rises from 0% to 100%. When the load reaches its peak during the test for the specimen with a 20% replacement ratio of RCA, the application speed of the load is not well controlled, leading to low ductility of the specimen, which is a test error.

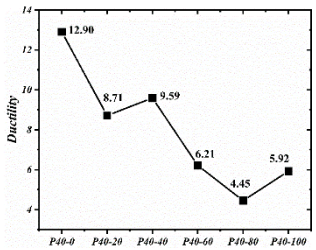

Fig. 12 Ductility

3.2.4. Strain analysis

The bottom or top of the mono column was where the specimens' maximum strain position occurred. This is essentially consistent with where each test specimen's maximum deformation occurred during the test procedure. Fig. 13 provides the lateral and longitudinal strain curves for each local measurement point of the specimens. The main test deformation points and the strain measurement points are both nearby. Analysis of the steel strain during the specimen's failure is possible. The steel is in the elastic stage at the initial loading stage, and the strain increased linearly with the eccentric load at that stage, according to the trend of the eccentric load-strain curve. Under an eccentric load, steel tubes underwent elastic deformation. The specimen started to experience significant deformation during the elastoplastic stage, and the steel's plasticity peaked. As a result, the eccentric load-strain curve's slope was reduced. Local yielding of the steel tube is earlier than specimen yielding when combined with specimen yielding load. The positions of the maximum lateral and longitudinal strains of the L-RACFST columns with various RCA replacement ratios are nearly identical, as shown in Fig. 13. Except for the specimens with a 60% RAC replacement ratio, the L-RACFST columns' maximum lateral and longitudinal strains all occurred at the same location. Even though there could have been some test errors, they also happened at the top of the specimen. The L-RACFST columns' maximum strain position matches the experimental phenomenon.

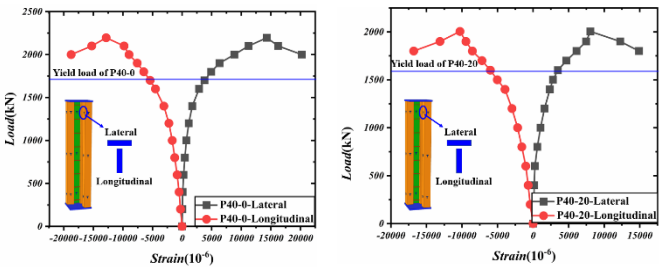

(a) P40-0 (b) P40-20

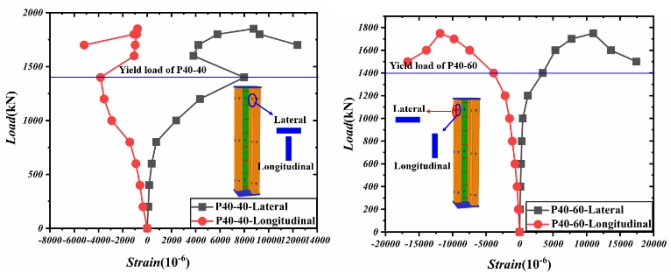

(c) P40-40 (d) P40-60

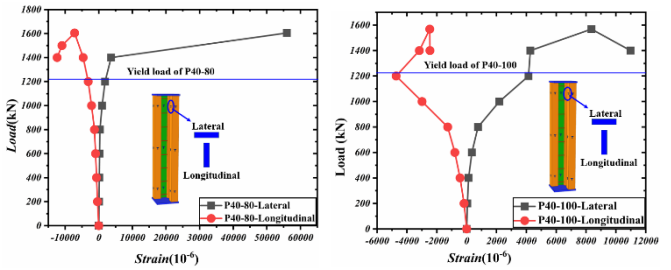

(c) P40-80 (d) P40-100

Fig. 13 The eccentric load–strain curve

3.2.5. The effect of the eccentricity

Reference [28], which the authors also published, contains the test results on L-RACFST columns with an 80mm loading eccentricity. In order to determine the impact of the eccentricity, the test results of specimens with a 40mm eccentricity were compared with the reference data. In Fig. 14, the comparison curve is displayed. It is evident that as eccentricity increases, the specimens' peak loads gradually decrease. This makes sense because a higher eccentricity corresponds to a higher bending moment and a lower axial load capacity.

Additionally, the specimens' stiffness curve gradually declines when the RCA replacement rate exceeds 40%. Although the ductility curve has no clear-cut law, when the replacement ratio of RCA is greater than 40%, the ductility generally decreases slowly. This is due to the test error of the specimen with a 20% replacement ratio of RCA.

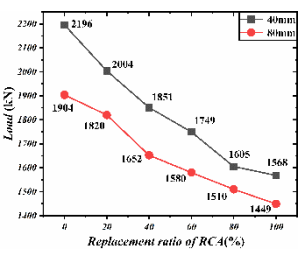

(a) Load comparison

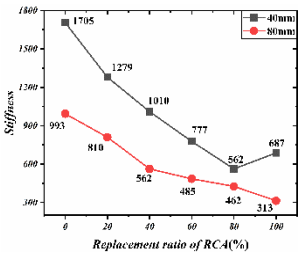

(b) Stiffness comparison

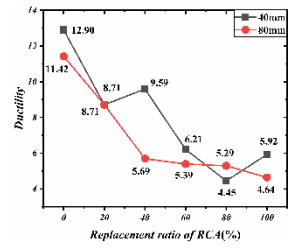

(c) Ductility comparison

Fig. 14 The comparison curve

4. Numerical simulation

4.1. Numerical models

The finite element analysis program ANSYS was used in this study to simulate the test procedure and the behaviors of the columns. The stiffeners, connection plates, and steel tubes were all modeled using SHELL181 elements. The RAC was modeled using SOLID65 details. Steel tubes and RAC adopted "surface to surface contact," which are TARGE170 and CONTAL173 elements. Due to the incomplete filling of the RAC, the production, and the transportation of the specimens, the initial imperfection of the specimens is the deviation from the ideal situation, which is caused by the initial bending and welding residual stress. In this study, the initial imperfection of the specimens is set at 1/1000 of the eigenvalue buckling analysis result. The modeled method cited an earlier source[28].Through mesh sensitivity analysis, in order to balance the calculation accuracy and speed, the SHELL181 elements size is determined as 10mm×10mm, and SOLID65 elements size is determined as 30mm×30mm×30mm.The friction coefficient adopted between the contact elements is 0.4[30]. All nodes' degrees of freedom in the X, Y, and Z directions were constrained at the bottom of the L-RACFST columns. All nodes had fixed X and Y degrees of freedom at the top of the L-RACFST columns. The finite element model is displayed in Fig. 15. In the modeling [31-33], the constraining effect of steel tubes on concrete was considered. The RCA of reference [34] constitutive relationship was used.

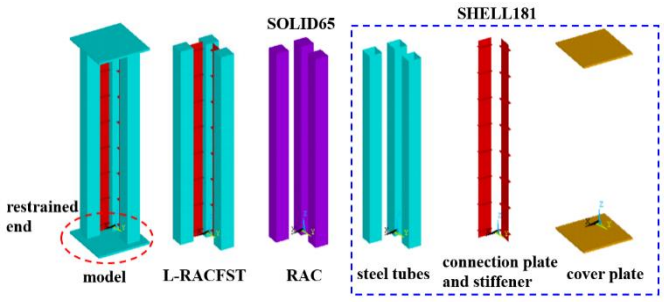

Fig. 15 Finite element models

4.2. The comparison of the failure mode

Fig. 16 depicts the comparison diagram of specimen failure modes. The failure modes of the specimens in both FEM and testing were similar and involved bending deformation of the specimens around the weak axis. The specimens' side mono columns (columns A and C) in FEM exhibit symmetrical deformation, and their side mono columns' deformation is greater than their corner mono columns' (column B). Additionally, the specimens' local buckling positions were comparable. It suggests that the failure mode of the test can be accurately simulated using the FEM.

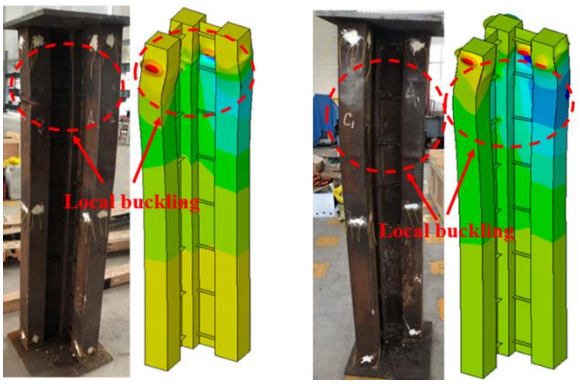

(a) P40-0 (b) P40-20

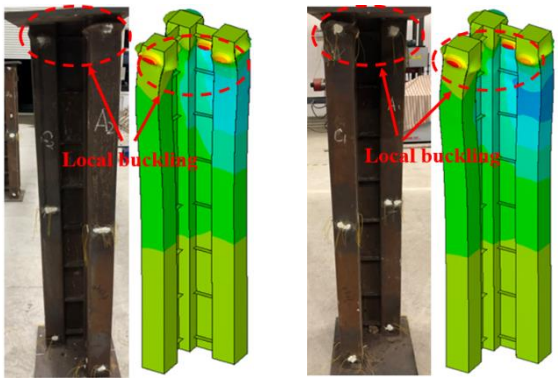

(c) P40-40 (d) P40-60

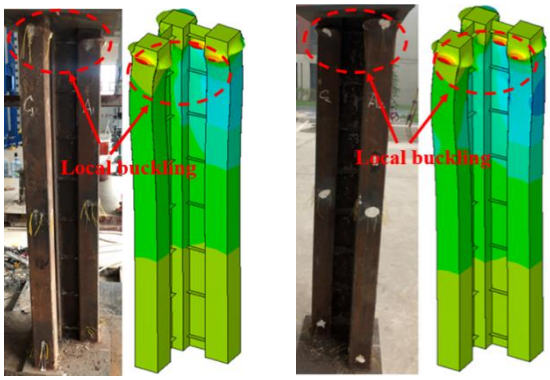

(e) P40-80 (f) P40-100

Fig. 16 Comparison of the failure mode

4.3. Bearing capacity comparison

Table 6
The load value information

Speci-mens	Yield load		$N_{y\text{-FEM}}/N_{y\text{-test}}$	Peak load		$N_{p\text{-FEM}}/N_{p\text{-test}}$
	$N_{y\text{-FEM}}$ (kN)	$N_{y\text{-test}}$ (kN)		$N_{p\text{-FEM}}$ (kN)	$N_{p\text{-test}}$ (kN)	
P40-0	1630	1722	0.95	2251	2196	1.03
P40-20	1568	1535	1.02	2095	2004	1.05
P40-40	1385	1363	1.02	1896	1851	1.02
P40-60	1353	1390	0.97	1781	1749	1.02
P40-80	1226	1236	0.99	1659	1605	1.03
P40-100	1191	1278	0.93	1617	1568	1.03
MV			0.98	*MV*		1.03

The load-displacement comparison curve is shown in Fig. 17. The specimen load value information is displayed in Table 6. As can be seen, the yield load and peak load average errors are within acceptable bounds at 0.98 and 1.03, respectively. These facts suggest that the numerical simulation technique used in this paper can accurately model the L-RACFST columns' capacity for eccentric compression.

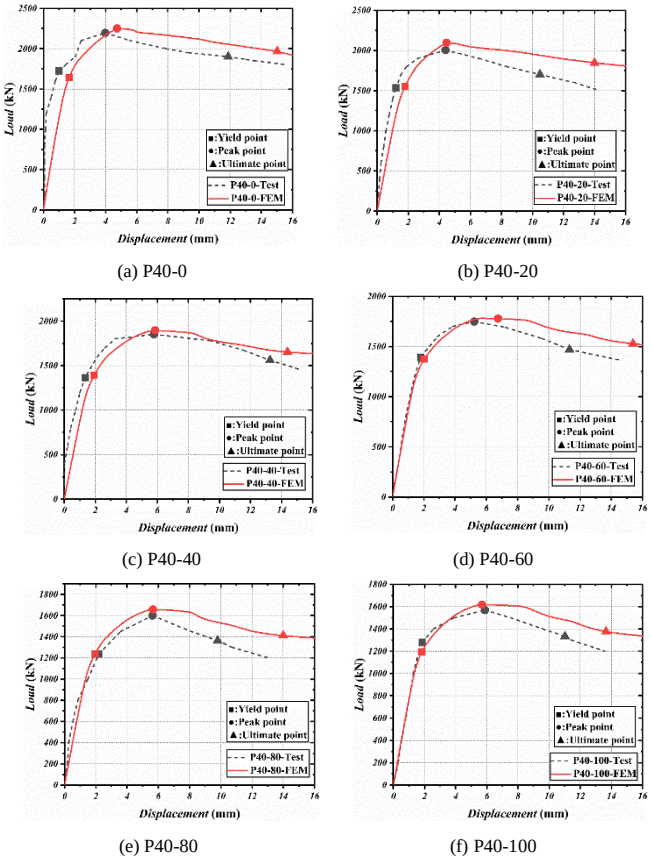

(a) P40-0 (b) P40-20

(c) P40-40 (d) P40-60

(e) P40-80 (f) P40-100

Fig. 17 Comparison of the load-displacement curve

5. Parametric analysis

5.1. The steel strengths effect

This section discusses the impact of the steel strength grades Q235, Q345, Q390, Q420, and Q460 on the specimens' bearing capacity. Fig. 18 depicts the load-steel strengths curve for the specimens. As steel strengths rise, the specimen's bearing capacity also gradually rises. The bearing capacity of the specimens increased by about 35% as steel strength increased from Q235 to Q460. This is because the stronger the steel's tensile strength, the stronger the steel tubes' restraint effect on the RAC, and the steel tubes' improved compressive strength, which increases the specimen's bearing capacity.

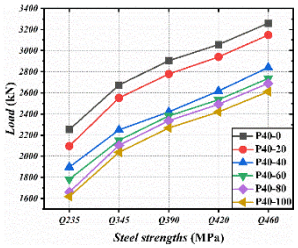

Fig. 18 Load-steel strengths curve

5.2. The steel ratio effect

In this paper, the steel thickness is changed to alter the steel ratio of the specimens. Equation (3) was used to define the steel ratio (D_r).

$$D_r = \frac{A_c}{A_s} \tag{3}$$

where, A_c denotes RAC area and A_s defines steel tube area.

When the steel ratio is altered, the steel tubes, connection plates, and stiffeners also change in thickness. The steel ratio of a mono column is calculated to be 14.44%, 28.60%, 41.48%, 53.08%, and 63.40%, respectively. The steel tubes have a thickness of 3.75, 7.75, 11.75, 15.75, and 19.75mm. The load-steel ratio curve of the specimens is shown in Fig.19 when the steel ratio varies. The bearing capacity of the specimens with replacement ratios of 0% and 100% increased by 175% and 282%, respectively, as the steel ratio increased from 14.44% to 63.40%. It is evident that the specimens' bearing capacity gradually increases as the steel ratio rises. This shows that the restraint effect of steel tubes on RAC is improved as steel tube thickness increases. This is because steel tubes get thicker, their restraining impact on the RAC becomes stronger, and their compressive strength increases, increasing the specimen's bearing capacity.

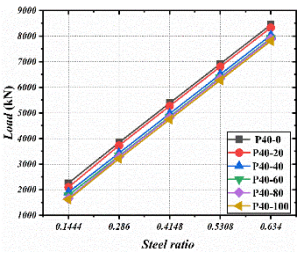

Fig. 19 Load- steel ratio curve

5.3. The effect of the connection plates width

The connection plates in this section are 100, 150, and 200 mm wide. Fig. 20 depicts the load-connection plate width curve. It is evident that the specimens' bearing capacity slightly increases as the connection plate's width increases. This suggests that the connection plate's primary function is to support the steel surface of its connecting surface and increase its stiffness, but that it has little bearing on improving the specimens' bearing capacity. This is because connecting plate width increases, and connecting plate thickness remains constant. This may result in a slight improvement in the stability of the connecting plate, which in turn may result in a slight improvement in the supporting effect of the connecting plate on the mono column, which in turn may result in a slight improvement in the carrying capacity of the L-RACFST columns.

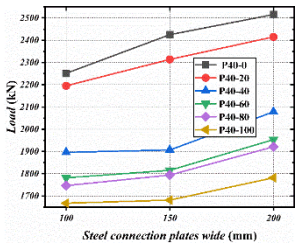

Fig. 20 Load- steel connection plates wide curve

6. Conclusions

Compared to a hollow L-shaped column, the eccentric compression behaviors of specimens with various RCA replacement ratios were investigated in the current research. The specimens' mechanical properties are simulated and examined using the validated numerical simulation. Following is an overview of the study's findings:

(1) Elastic stage, elastoplastic stage, and plastic stage under eccentric load were the three stages of the L-RACFST columns' testing procedure. The specimens tend to enter the plastic stage instantly, revealing a lower degree of ductility when the RCA replacement ratio is greater than 40%. The overall instability failure of the L-RACFST columns is the ultimate failure, and the replacement ratio of RCA has little bearing on the ultimate failure mode. Localized buckling inward and outward of the steel tubes leads to the failure mode of the hollow L-shaped column.

(2) The specimens' bearing capacity decreases with an increase in the replacement ratio of RCA. The specimens' bearing capacity degrades more quickly when the RCA replacement ratio exceeds 40%. The specimen with a replacement ratio of 100% has a bearing capacity reduction of about 29% compared to the specimen with a replacement ratio of 0%.

(3) The L-RACFST columns' ductility and stiffness gradually decline as RCA's replacement ratio rises; the decline rate is slower when RCA's replacement ratio is higher than 40%. The ductility coefficient decreased by 54%, and the stiffness coefficient decreased by 60% as the replacement ratio of RCA increased from 0% to 100%.

(4) As eccentricity rises, the L-RACFST columns' bearing capacity gradually declines. This is also supported by the research findings of reference [28].

(5) Although the connection plate increases the stiffness of the steel tubes, this has little impact on the specimens' ability to support more weight. The L-RACFST columns' bearing capacity can be enhanced by using the engineering design technique of increasing steel strength and ratio. It is not advised to make the connection plate wider to improve the bearing capacity of the specimens.

(6) When taken into account with the reference [28], it is preferable in engineering for the replacement ratio of RCA in the L-RACFST columns to be lower than 40%.

References

[1] Etxeberria M , E Vázquez, A Marí, et al. influence of amount of recycled coarse aggregates and production process on properties of recycled aggregate concrete[J]. Cement & Concrete Research, 2007, 37(5):735-742.

[2] Corinaldesi V , Moriconi G . Influence of mineral additions on the performance of 100% recycled aggregate concrete[J]. Construction & Building Materials, 2009, 23(8):2869-2876.

[3] Xiao J Z , Jia-Bin L I , Sun Z P , et al. Study on Compressive Strength of Recycled Aggregate Concrete[J]. Journal of Tongji University, 2004, 32(12):1558-1561.

[4] Olek, Jan, Behnood, et al. Predicting modulus elasticity of recycled aggregate concrete using M5 ' model tree algorithm[J]. Construction and Building Materials, 2015.

[5] Wdeeing P A，Rasheeduzzafar，Khan A. Recycied concrete-a source for new aggregate. Cement Concrete and Aggregates，1984，6（1）：17-23.

[6] Ridzuan A R M, Ibrahim A, Ismail A M M, et al. Durablity performance of recycled aggregate concrete. Achieving Sustainability in Construction,2005(7):193–202.

[7] Huda S B , Alam M S . Mechanical and Freeze-Thaw Durability Properties of Recycled Aggregate Concrete Made with Recycled Coarse Aggregate[J]. Journal of Materials in Civil Engineering, 2015, 27(10):04015003.

[8] Mahmood W , Khan A U R , Ayub T . Mechanical and Durability Properties of Concrete Containing Recycled Concrete Aggregates[J]. Iranian Journal of Science and Technology, Transactions of Civil Engineering, 2021:1-20.

[9] Shi X S , Wang Q Y , Qiu C C , et al. Experimental Study on the Properties of Recycled Aggregate Concrete with Different Replacement Ratios from Earthquake-stricken Area[J]. Journal of Sichuan University(Engineering ence Edition), 2010, 42:170-176.

[10] Huang Y , Xiao J . Seismic behavior and damage assessment of recycled aggregate concrete-filled steel tube columns[J]. Tongji Daxue Xuebao/Journal of Tongji University, 2013, 41(3):330-335+354.

[11] Mohanraj E K , Kandasamy S , Malathy R . Behaviour of steel tubular stub and slender columns filled with concrete using recycled aggregates[J]. Journal of the South African Institution of Civil Engineering, 2011, 53(2):31-38.

[12] A W L , B Z L A , C Z T , et al. Mechanical behavior of recycled aggregate concrete-filled steel tube stub columns after exposure to elevated temperatures - ScienceDirect[J]. Construction and Building Materials, 2017, 146:571-581.

[13] Liu W , Cao W , Zhang J , et al. Mechanical Behavior of Recycled Aggregate Concrete-Filled Steel Tubular Columns before and after Fire[J]. Materials, 2017, 10(3):274.

[14] Liu, Feng, Liao, et al. Seismic performance of recycled aggregate concrete-filled steel tube columns[J]. Journal of Constructional Steel Research, 2017.

[15] Dong J F , Wang Q Y , Guan Z W . Structural behaviour of recycled aggregate concrete filled steel tube columns strengthened by CFRP[J]. Engineering Structures, 2013, 48:532-542.

[16] Chen Z P , Chen X H , Ke X J , et al. Experimental study on the mechanical behavior of recycled aggregate coarse concrete-filled square steel tube column. IEEE, 2010.

[17] Wang Y , Jie C , Yue G . Testing and analysis of axially loaded normal-strength recycled aggregate concrete filled steel tubular stub columns[J]. Engineering Structures, 2015, 86(mar.1):192-212.

[18] Tang Y C , Li L J , Feng W X , et al. Seismic performance of recycled aggregate concrete–filled steel tube columns[J]. Journal of Constructional Steel Research, 2017, 133:112-124.

[19] Chen Z H , Rong B , Fafitis A . Axial compression stability of a crisscross section column composed of concrete-filled square steel tubes[J]. Journal of Mechanics of Materials and Structures, 2010, 4(10):1787-1799.

[20] B. Rong, Z. Chen, A. Fafitis, N. Yang. Axial Compression Behavior and Analytical Method of L-Shaped Column Composed of Concrete-Filled Square Steel Tubes[J]. Transactions of Tianjin University, 2012(03):180-187.

[21] Chen Z , Rong B . Research on axial compression stability of L-shaped column composed of concrete-filled square steel tubes[J]. Building Structure, 2009.

[22]B. Rong, Z. Chen, T. Zhou. Research on axial compression strength of L-SHAPED short column composed of concrete-filled square steel tubes[J].Industrial Construction 2009, 39(11), 104.

[23] Zhou T,Chen Z ,Liu H. Seismic behavior of special shaped column composed of concrete filled steel tubes[J]. Journal of Constructional Steel Research, 2012, 75(75):131-141.

[24] Xu M , Zhou T , Chen Z , et al. Experimental study of slender LCFST columns connected by steel linking plates[J]. Journal of Constructional Steel Research, 2016, 127(DEC.):231-241.

[25] Xiong Q , Chen Z , Zhang W , et al. Compressive behaviour and design of L-shaped columns fabricated using concrete-filled steel tubes[J]. Engineering Structures, 2017, 152(dec.1):758-770.

[26] Liu J , Zhou T , Lei Z , et al. Eccentric compression performance of slender L-shaped column composed of concrete-filled steel tubes connected by steel linking plates[J]. Journal of Constructional Steel Research, 2019, 162(Nov.):105675.1-105675.16.

[27] Chen Z , Liu J , Zhou T , et al. Uniaxial Eccentric-Compression Performance Analysis for Double-Plate Connected Concrete-Filled Steel-Tube Composite Columns[J]. Journal of Structural Engineering, 2020, 146(8):04020161.

[28] Ma,T.;Chen,Z.;Du,Y.;Zhou,T.;Zhang,Y.Mechanical Properties of L-Shaped Column Composed of RAC-Filled Steel Tubes under Eccentric Compression .Metals2022,12,953. https://doi.org/10.3390/met12060953

[29] GB/T 50081-2019, Standard for test methods of concrete physical and mechanical properties, Standardization Administration of China, 2019.

[30] Du Y , Zhang Y , Chen Z , et al. Axial compressive performance of CFRP confined rectangular CFST columns using high-strength materials with moderate slenderness[J]. Construction and Building Materials, 2021, 299(4):123912.

[31] Yang Y, Han L. Compressive and flexural behaviour of recycled aggregate concrete filled steel tubes (RACFST) under short-term loadings[J].Steel & Composite Structures,2006, 6 (3): 257-284.

[32] Yang Y. Theoretical research on load-deformation relations of recycled aggregate concrete-filled steel tubular members[J]. Industrial Construction,2007, 37 (012): 1-6.

[33] Xiao J, Lan Y. Investigation on the Tensile Behavior of Recycled Aggregate Concrete [J].Journalof building materials,2006 (02): 154-158.

[34] Li J,Chen Z,Du Y,et al.Study on constitutive model of core concrete of recycled aggregate concrete filled steel tubular columns under compression[J].Industrial Construction, 2021,51(05):108-115+15.